Hair follicle stem cell progeny heal blisters while pausing skin development

Yu Fujimura[1], Mika Watanabe[1,2], Kota Ohno[3], Yasuaki Kobayashi[3], Shota Takashima[1], Hideki Nakamura[1], Hideyuki Kosumi[1], Yunan Wang[1], Yosuke Mai[1], Andrea Lauria[2,4], Valentina Proserpio[2,4], Hideyuki Ujiie[1], Hiroaki Iwata[1], Wataru Nishie[1], Masaharu Nagayama[3,5], Salvatore Oliviero[2,4], Giacomo Donati[2], Hiroshi Shimizu[1], Ken Natsuga[1]*

[1]Department of Dermatology, Hokkaido University Graduate School of Medicine, Sapporo, Japan

[2]Department of Life Sciences and Systems Biology, Molecular Biotechnology Centre, University of Turin, Turin, Italy

[3]Research Institute for Electronic Science, Hokkaido University, Sapporo, Japan

[4]Italian Institute for Genomic Medicine, Candiolo (TO), Italy

[5]Japan Science and Technology Agency, CREST, Kawaguchi, Japan

Conflict of Interest

The authors declare that no conflict of interest exists.

20 *Correspondence and reprint requests to:

21 Ken Natsuga, M.D., Ph.D.

22 Department of Dermatology, Hokkaido University Graduate School of Medicine

23 North 15 West 7, Sapporo 060-8638, Japan

24 Telephone: +81-11-716-1161, ext. 5962

25 E-mail: natsuga@med.hokudai.ac.jp

26

Abstract

Injury in adult tissue generally reactivates developmental programs to foster regeneration, but it is not known whether this paradigm applies to growing tissue. Here, by employing blisters, we show that epidermal wounds heal at the expense of skin development. The regenerated epidermis suppresses the expression of tissue morphogenesis genes accompanied by delayed hair follicle (HF) growth. Lineage tracing experiments, cell proliferation dynamics, and mathematical modeling reveal that the progeny of HF junctional zone stem cells, which undergo a morphological transformation, repair the blisters while not promoting HF development. In contrast, the contribution of interfollicular stem cell progeny to blister healing is small. These findings demonstrate that tissue development can be sacrificed for the sake of wound regeneration and suggest that tissue repair does not coincide with the reactivation of developmental programs in all regenerative contexts. Our study elucidates the key cellular mechanism of wound healing in skin blistering diseases.

Keywords

Wnt signaling, epidermal stem cells, epidermolysis bullosa, basement membrane zone

Introduction

Tissue responds to injury by transforming its cellular components and extracellular matrix from homeostasis into a regenerative state. Damaged tissue typically reactivates an embryonic gene program in epithelia to accelerate tissue regeneration (1-4). However, it is unknown whether this phenomenon also applies to injuries in developing tissue, in which the embryonic gene expression program is switched on before damage.

The epidermis is a stratified epithelium of the skin and is located on the surface of the body, where it serves as a barrier against external stimuli and microorganisms (5). Cellular proliferation and differentiation in the epidermal basal layer, where epidermal stem cells (SCs) are present, are fine-tuned to maintain the integrity of the epidermis (6). The epidermis attaches to the dermis through proteins in the epidermal basement membrane zone (BMZ) (7). Epidermal BMZ proteins function as a niche for epidermal SCs (8), and the loss of these proteins, such as α6 integrin (ITGA6), β1 integrin, and collagen XVII (COL17), leads to transient epidermal proliferation (9-11).

Skin wounding causes pain and carries a significant risk of bacterial infection. The sources of skin wound healing have been extensively investigated in experimental animals (12, 13). Hair follicles (HFs), epidermal appendages, fibroblasts, and immune cells coordinate to heal the wound, and the contribution of each component can vary depending on the assay (14). Wounding in adult skin induces the expression of genes regulating epidermal development, including SOX11 and SOX4 (1).

Conventional skin wounding assays have employed full-thickness skin wounds, in which all skin components are removed, including the epidermis, epidermal appendages, dermis, and subcutaneous fat tissue. In contrast to conventional full-

thickness skin wounds, epidermal detachment, as exemplified by subepidermal blisters, is distinctive because it does not affect the structures below the epidermis per se. The epidermis is detached from the dermis in several pathological conditions, such as burns (15), congenital defects in epidermal BMZ proteins (epidermolysis bullosa (EB)) (16, 17), autoimmunity to these proteins (pemphigoid diseases) (18), and severe drug reactions, such as Stevens-Johnson syndrome/toxic epidermal necrolysis (19). Although the cells that contribute to the repair of full-thickness skin wounds have been identified (13, 20-24), the cellular dynamics of subepidermal blister healing are completely unknown. In addition, full-thickness skin wounding, when applied to developmental skin, is unsuitable for distinguishing tissue regeneration and development. In contrast, blistering injury allows us to monitor both skin regeneration (reepithelization of the epidermis) and morphogenesis (HF development) within the same wound bed.

Here, by taking advantage of subepidermal blisters, we explore the effects of injury on developmental tissue. Unexpectedly, blistering injury is found to reduce the expression of tissue morphogenesis genes in the healed epidermis and to direct HFSCs, rather than epidermal SCs, to provide progeny to heal the wound and to suspend HF development.

Results

Subepidermal blister formation and its healing process

The suction-blister technique was developed more than a half-century ago to selectively remove the epidermis from the dermis (25, 26), and it has been utilized to harvest epidermal pieces for transplant to repair human skin defects. We reasoned that suction blisters on neonatal mice, in which the epidermis is removed while HFs, the dermis, and subcutaneous fat tissues are maintained in the wounds, enable us to examine the direct relationship between tissue injury and skin development. Therefore, we applied constant negative pressure to the dorsal skin of C57BL/6 wild-type (WT) neonates to produce subepidermal blisters (postnatal day 1 (P1), **Figure 1a**). Histologically, skin separation occurred at the level of the dermoepidermal junction (DEJ) (**Figure 1b**). HFs, as shown by alkaline phosphatase (AP)-positive dermal papillae, remained on the dermal side of the blisters (**Figure 1b**). Dermis and subcutaneous tissues were intact after blistering (**Figure 1b**). α6 integrin (ITGA6), a hemidesmosome protein, was seen at the blister roof, whereas type IV collagen (COL4), a major component of the epidermal basement membrane, and laminin 332 (L332) were present at the base of the blister (**Figure 1c**). In line with the immunofluorescence data, hemidesmosomes localized on the blister roof and lamina densa (basement membrane) were observed at the blister base by electron microscopy (**Figure 1d**), as seen in human suction blisters (25) and their murine counterparts (27).

We then characterized the healing processes of the subepidermal blisters. One to two layers of the regenerated epidermis, marked with pan-cytokeratin, was found one day after blister formation (P2, **Figure 1e**). The regenerated epidermis restored ITGA6

111 expression at the DEJ (**Figure 1e**). The shape of the basal keratinocytes in the intact
112 skin was cuboidal or columnar (P2, keratin 14 (K14)-positive cells in the nonlesional
113 area, **Figure 1f**). In contrast, the regenerated keratinocytes in the blistered skin
114 transformed from cuboidal to a wedge/flattened shape (P2, K14-positive cells in the
115 lesional area, **Figure 1f**) (27). Two days after blistering (P3), the stratified epidermal
116 layers were mostly restored but still lacked loricrin-positive granular layers, a hallmark of
117 proper epidermal differentiation, in the lesional area (**Figure 1g**). The final step in
118 epidermal differentiation was completed by the formation of loricrin-positive granular
119 layers three days after blister formation (P4, **Figure 1h**). These results demonstrate that
120 subepidermal blisters on neonates can serve a model for visualizing wound healing
121 without damaging HFs and other dermal components at the developmental stage.
122

123 **Epidermal restoration at the expense of skin development**

124 To elucidate the effects of the blistering injury on the neonatal skin, we performed RNA-
125 seq profiling of the regenerated epidermis one day after blistering (P2, **Figure 2a**).
126 Unexpectedly, the expression of genes involved in HF morphogenesis, such as Wnt
127 signaling, melanogenesis, and Hedgehog signaling, was downregulated (**Figure 2b,**
128 **2c**), suggesting that epidermal wounding tunes down tissue development to accelerate
129 blister healing. In agreement with this hypothesis, the number of hair canals, which are
130 present in only developed HFs (HF morphogenesis, stage 6-8) (28), was reduced in the
131 regenerated epidermis (**Figure 2d, 2e**). HF growth under the regenerated epidermis at
132 P4 was delayed at stages 5 and 6, whereas the surrounding intact skin of the blisters or
133 the normal skin of the littermate controls had stage 7 HFs (**Figure 2f**). In Wnt-reporter

134 mice (ins-Topgal+), the LacZ-positive area that is indicative of active Wnt signaling was
135 diminished upon blister formation, accompanied by smaller HFs than those in the
136 surrounding intact skin (P2, **Figure 2g**).

137 The expression of genes involved in cytokine-cytokine receptor interactions and
138 chemokine, TNF, IL-17, and JAK-STAT signaling pathways was increased in the
139 regenerated epidermis (**Figure 2b, 2c**), and these pathways are implicated in the
140 recruitment of immune cells. However, the number of neutrophils, lymphocytes, and
141 macrophages was not increased in the lesional dermis (P2, **Supplementary Figure 1a-**
142 **c**), in which 1-2 layers of the regenerated epidermis covered the wound one day after
143 blistering, suggesting that the immune cells might play a minimal role in the context of
144 blister healing because of the fast regeneration process (<24 hr).

145 These data indicate that, in the context of skin morphogenesis where the immune
146 system is not yet fully defined, subepidermal blisters heal at the expense of HF growth.

147

148 **Progeny of junctional zone SCs represent the main cellular contribution to blister**
149 **healing**

150 Wounded lesions require epithelial cell proliferation and migration to restore skin
151 integrity. We then investigated the dynamics of epidermal and HF keratinocytes during
152 blister healing. One day after blister formation (P2), BrdU+ cells were abundant in the
153 HFs and the intact epidermis adjacent to the blisters (**Figure 3a**). Cells positive for α5
154 integrin (ITGA5), a marker of migrating keratinocytes (23), were seen in the HFs within
155 the lesional area and in the epidermal boundary between the blister and the nonlesional
156 area (epidermal tongue) (**Figure 3b**). As HF growth was delayed in the regenerated

157 epidermis (**Figure 2d-g**) and proliferative cells were abundant in HFs of the lesional
158 area (**Figure 3a**), HF keratinocytes were deduced to participate in epidermal
159 regeneration rather than in HF development.
160 To confirm this hypothesis, we employed a short-term lineage tracing strategy with
161 suction blistering (**Figure 3c**). K14-lineage labeled cells (K14CreER:R26R-H2B-
162 mCherry or K14CreER:R26R-confetti), mainly progeny of SCs in the interfollicular
163 epidermis (IFE), were sparse in the regenerated epidermis (**Figure 3d, 3e**). In contrast,
164 most of the cells in the regenerated epidermis were Lrig1 (leucine-rich repeat and
165 immunoglobulin-like domain protein 1)-lineage labeled cells (Lrig1CreER:R26R-H2B-
166 mCherry or Lrig1CreER:R26R-confetti), which are the progeny of junctional zone SCs
167 (**Figure 3f, 3g**). These data indicate that the HF junctional zone on the dermal side of
168 the blister is the main pool for the keratinocytes that heal subepidermal blisters while
169 halting HF development.
170
171 **Depletion of HF junctional stem cells from the wound bed of the blisters**
172 **promotes the contribution of IFESC progeny to blister healing**
173 The contribution of junctional zone HFSC progeny to blister healing led us to investigate
174 how the epidermis regenerates in the absence of HFs at the blister base (dermis). Type
175 XVII collagen (COL17) is expressed not only in the IFE but also in the bulge region of
176 the HFs (**Figure 4a**) (11, 29-32). COL17 is encoded by the *COL17A1* gene, and its
177 deficiency leads to junctional EB (33). The splitting of neonatal *Col17a1*$^{-/-}$ (34) dorsal
178 skin upon suction blistering was observed between ITGA6 and COL4/L332 (**Figure 4b,**
179 **4c**), as was the case in wild-type neonates (**Figure 1c, 1d**). Intriguingly, suction

180 blistering (**Figure 1a**) of *Col17a1*$^{-/-}$ dorsal skin detached HFs from the dermis (P1,
181 **Figure 4d**). In agreement with this finding, dermal papilla cells (AP+) were observed on
182 the roof side of the blisters of *Col17a1*$^{-/-}$ mice, whereas the blister roofs of control mice
183 did not have these cells (P1, **Figure 4e**). Epidermal regeneration was not apparent in
184 *Col17a1*$^{-/-}$ mice one day after suction blistering (P2), whereas the control mice showed
185 regeneration of the epithelial layers (**Figure 4f**). *Col17a1*$^{-/-}$ mice had delayed expression
186 of loricrin in the regenerated epidermis three days after blister formation (P4, **Figure 4f**).
187 BrdU+ cells were abundant in the *Col17a1*$^{-/-}$ mouse epidermis surrounding blisters as
188 was the case for controls (**Figures 3a, 4g**). Lineage tracing experiments (**Figure 3c**)
189 revealed that IFESC progeny covered most of the regenerated area (K14CreER:R26R-
190 H2B-mCherry:*Col17a1*$^{-/-}$) at P4 (**Figure 4h, 4i**). The transgenic rescue of *Col17a1*$^{-/-}$ by
191 overexpressing human COL17 (hCOL17+;*Col17a1*$^{-/-}$) (34) normalized blister healing
192 (P4, **Supplementary Figure 2**). These data demonstrate that upon HF depletion, the
193 IFE can compensate the lack of junctional stem cells and repair defects in the
194 epidermis.
195
196 **Impaired flattening of regenerated keratinocytes delays blister healing**
197 We further sought to identify other modulators of subepidermal blister healing. We
198 first focused on collagen VII (COL7), encoded by *Col7a1*. COL7 forms anchoring fibrils
199 and is located at the DEJ (**Figure 5a**) but just below the basement membrane (35, 36),
200 and its deficiency leads to dystrophic EB (37, 38). As conventional wound healing is
201 delayed in COL7-hypomorphic mice (39), we applied the suction-blister method to
202 *Col7a1*$^{-/-}$ mice (40) (**Figure 5b-h, Supplementary Figure 3**). In contrast to that in WT

203 and *Col17a1*$^{-/-}$ suction blisters (**Figure 1c, 1d, 4b, 4c**), skin splitting occurred at the level
204 below the basement membrane in *Col7a1*$^{-/-}$ mouse dorsal skin, as shown by the
205 presence of L332 and COL4 on the blister roof epidermis (P1, **Figure 5b, 5c**). The
206 epidermal defects were not repaired in *Col7a1*$^{-/-}$ mice, whereas the epidermis of the
207 control blistered skin regenerated one day after blistering (P2, **Figure 5f,**
208 **Supplementary Figure 3**), which is consistent with the delayed healing of full-thickness
209 skin wounds in COL7-hypomorphic mice (39). This finding is contrasted by the fact that
210 COL7-depleted keratinocytes migrate faster than WT keratinocytes in vitro (41, 42). We
211 examined the HFs of *Col7a1*$^{-/-}$ mice to explain the slowed epidermal regeneration
212 because HFs are the main contributor to blister healing (**Figure 2a-g**). However, HFs
213 were present in the *Col7a1*$^{-/-}$ mouse wound bed (blister base) (P1, **Figure 5d, 5e**) as
214 opposed to that of *Col17a1*$^{-/-}$ mouse (P1, **Figure 4d, 4e**). Moreover, the number of
215 BrdU+ cells in HFs was comparable between *Col7a1*$^{-/-}$ and control mice (P2, **Figure 5g**,
216 **Supplementary Figure 3**), suggesting that the proliferation of HF keratinocytes does
217 not account for the delayed blister healing of *Col7a1*$^{-/-}$ mice.
218 Second, we treated the blistered skin in wild-type mice with extracellular calcium
219 (**Figure 5i-k**, **Supplementary Figure 3**). Extracellular calcium is a potent inhibitor of
220 proliferation and migration in cultured keratinocytes as well as an inducer of
221 differentiation (43, 44). Consistent with previous in vitro assays, the intrablister
222 administration of $CaCl_2$ (1.8 mM or 9.0 mM) just after suction blistering delayed
223 epidermal regeneration in vivo (P2, **Figure 5i**). Premature differentiation, which might
224 hinder wound healing, was not apparent in the $CaCl_2$-treated blisters, as K10 labeling
225 was seen only at the blister roof but not in the keratinocytes on the wound bed (P2,

226 **Figure 5i**). Similar to that in *Col7a1*$^{-/-}$ mouse blisters, the number of BrdU+ cells in HFs
227 was not reduced in $CaCl_2$-treated blisters (P2, **Figure 5j**, **Supplementary Figure 3**).
228 These two examples strongly suggest that there are factors other than HF
229 keratinocyte proliferation that modulate blister healing. During blister healing,
230 keratinocytes reshape into a wedge-shaped morphology (**Figure 1f**), which is mirrored
231 by the RNA-seq data showing that the expression of genes involved in the regulation of
232 the actin cytoskeleton is decreased in the regenerated epidermis (**Figure 2b, 2c**).
233 Wedge-shaped/flattened keratinocytes are believed to be superior to cuboidal/columnar
234 keratinocytes for covering epidermal defects. In the intact (nonblistered) skin, the
235 morphology of *Col7a1*$^{-/-}$ or Ca-treated basal keratinocytes was similar to that of control
236 cells (P2, the nonlesional area in **Figure 5f, 5h, 5i, 5k**). The regenerated keratinocytes
237 became wedge-shaped/flattened in the control group, as shown in **Figure 1f**. However,
238 the keratinocytes in the regenerated epidermis of *Col7a1*$^{-/-}$ or Ca-treated mice were not
239 as flat as those of control mice but were still rather cuboidal (P2, the lesional area in
240 **Figure 5f, 5h, 5i, 5k**), which, at least partly, explains the delayed blister healing in these
241 mice. These data imply that morphological changes in keratinocytes contribute to
242 subepidermal blister healing.
243
244 **Mathematical modeling reproduces blister healing**
245 These in vivo experiments led us to speculate that HF/IFE cell proliferation during
246 paused HF development and the morphological changes of the regenerated
247 keratinocytes might simply account for the dynamics of subepidermal blister healing. To
248 answer this question, we employed mathematical modeling. The particle-based model

249 of self-replicating cells (45, 46) allowed us to visualize the dynamics of the epidermal
250 basal layer and to establish the epidermal defects on the basement membrane. We
251 utilized the data on the number of BrdU+ cells among HF vs. IFE keratinocytes
252 (approximately 7:1 per unit of epidermal length; **Figure 3a**) and on the shape of the
253 regenerated vs. normal keratinocytes (2:1 the length of the major cell axis; **Figure 5h,**
254 **5k**). SC progeny within the epidermal defects (colored in red), simulating HF-derived
255 cells, had a more substantial contribution to wound healing than IFE SCs (colored in
256 yellow; **Figure 6a, 6b, Supplementary Video 1**), as seen in the lineage tracing
257 experiments (**Figure 3c-g**). The absence of SCs within the epidermal defects,
258 simulating HF depletion in the wound bed, showed delayed healing (**Figure 6c, 6d,**
259 **Supplementary Video 2**), in agreement with *Col17a1*$^{-/-}$ epidermal regeneration results
260 (**Figure 4e-g**). A less flattened morphology of the regenerated keratinocytes, simulating
261 *Col7a1*$^{-/-}$ and Ca-treated blister healing (regenerated vs. normal keratinocytes, 1.3-1.6:1
262 in length; **Figure 5h, 5k**), slowed epidermal regeneration (**Figure 6e, 6f,**
263 **Supplementary Video 3**). These in silico data demonstrate that the contribution of
264 HFSC progeny and the morphological change in the regenerated keratinocytes are
265 sufficient to recapitulate the in vivo subepidermal blister healing.
266 We finally asked whether this HF contribution to wound healing could be applied to a
267 human setting, in which HFs are larger but much more sparsely distributed than their
268 murine counterparts (**Supplementary Table 1**). Mathematical modeling revealed that
269 the progeny of HF keratinocytes are still the main contributors to subepidermal blister
270 healing in humans (**Supplementary Figure 4a, b, Supplementary Video 4**). To further
271 confirm the in silico modeling results, we examined human subepidermal blister

272 samples and found that epidermal regeneration by HFs was observed in the samples
273 with the re-epithelized area (**Supplementary Figure 4c**). These findings strongly
274 suggest that HFs can replenish keratinocytes for subepidermal blister healing in both
275 mice and humans.
276

Discussion

Although recent studies have reported that injury causes damaged tissue to shift to an embryonic-like state, there is a poor understanding of how regeneration affects development at the damaged tissues. Here, we applied the blistering injury to neonatal mouse dorsal skin and showed the skewed contribution of HFSC progeny to wound healing rather than HF development.

Previous studies on skin wounding combined with the fate mapping of murine skin delineated the involvement of epithelial, mesenchymal, and immune cells in wound healing, depending on different settings (12, 13). However, as full-thickness skin wounds, even when they are applied to neonatal skin, remove all skin components, it is challenging to see the effects of development on injury or vice versa. Our blistering injury has an advantage over conventional skin wounding studies in that only the epidermis is removed by constant negative pressure, with the other skin components and basement membrane being retained in the wounds, which allowed us to examine “pure” epidermal wound healing processes during skin development. Our study contrasts with wound-induced embryonic gene expression (1) and follicular neogenesis upon full-thickness skin wounding in adult (47, 48) and neonatal mice (49). It is noteworthy that subepidermal blister healing suppressed Wnt signaling in our study (**Figure 2a-2g**), whereas Wnt activation has been implicated in full-thickness skin wounds (48), implying context-dependent Wnt activities in tissue regeneration.

Previous studies have suggested the possible involvement of HFs in epidermal regeneration in human suction blisters (50) and extracellular matrix alterations in the skin-split area (51, 52). We show that the progeny of HF junctional zone SCs mainly

300 repair subepidermal blisters (**Figures 3f, 3g, 6a, 6b**). However, the IFE can also serve
301 as a reservoir of keratinocytes to repair epidermal defects when HFs are depleted
302 (**Figure 4h**). How the contribution of two sources of keratinocytes to blister healing is
303 regulated is unknown, but the significant contribution of HF junctional zone progeny is
304 reasonable because HFs are densely located in the wound bed (blister base). In
305 contrast, the progeny of IFESCs could recover only from the blister edge, as
306 demonstrated by mathematical modeling (**Figures 3d-3g, 6a, 6b**). The role of HFSCs is
307 also highlighted by delayed HF growth in the regenerated epidermis, as corroborated by
308 the downregulated Wnt signaling (**Figure 2a-2g**). These findings indicate that there is a
309 coordinated balance between tissue development and wound healing, which has not
310 been well recognized. In addition, the expression of IL-17 signaling pathway genes was
311 increased, although the recruitment of immune cells was not evident one day after
312 blistering (**Supplementary Figure 1**). Recently, IL-17 signaling has been shown to drive
313 Lrig1-lineage cell recruitment in wound healing and tumorigenesis (53). Therefore, IL-17
314 signaling might also help Lrig1-lineage cells translocate from HFs to repair epidermal
315 defects in our study (**Figure 3f, 3g**).
316 The dynamics of cytoskeletal changes directly affect cellular morphology and
317 migration potential (54). Previous studies have shown that cells undergo a
318 morphological transformation into a wedge/flattened shape at the leading edge of
319 migrating cells (55) and in regenerated keratinocytes during wound healing (27, 56).
320 Our study has shed further light on the significant impact of the keratinocyte
321 morphological changes on in vivo wound healing through blistering experiments in

322 *Col7a1*$^{-/-}$ and Ca-treated mice and mathematical modeling (**Figure 5f, 5h, 5i, 5k, 6a, 6e,**
323 **6f**).
324 Our in vivo blistering experiments can mimic and replace the in vitro cultured cell
325 wound healing assay (e.g., scratch wounding), which has been used in the field of cell
326 biology for decades because subepidermal blisters are epidermal wounds and the
327 involvement of mesenchymal and immune cells are not pivotal for blister healing. In vivo
328 intrablister administration of drugs, as exemplified by extracellular calcium
329 administration (**Figure 5i**), could be an alternative to in vitro chemical treatment of
330 scratch-wounded cultured cells to develop new therapeutic options for wound healing,
331 especially of subepidermal blisters.
332 Our in vivo suction-blister model recapitulates the human pathological epidermal
333 detachment seen in EB, pemphigoid diseases, burns, and severe drug reactions such
334 as Stevens-Johnson syndrome/toxic epidermal necrolysis. Loss-of-function mutations in
335 *COL17A1* (33) and *COL7A1* (37, 38) lead to junctional and recessive dystrophic EB in
336 humans, respectively. Therefore, *Col17a1*$^{-/-}$ and *Col7a1*$^{-/-}$ mouse blistering also serves
337 as an EB wound model. The prominent hair loss in human *COL17A1*-mutated junctional
338 EB might be reflected by the depletion of HFs from the wound bed in *Col17a1*$^{-/-}$ blisters
339 (**Figure 4d, 4e**), whereas the hair loss in recessive dystrophic EB is not as severe as
340 that in the junctional subtype (57), consistent with the maintenance of HFs in the dermis
341 of *Col7a1*$^{-/-}$ mouse dorsal skin upon suction blistering (**Figure 5d, 5e**). Furthermore, the
342 processes of subepidermal blister healing highlight HFs as a target for treating the
343 wounds of EB and other blistering diseases.

344 In closing, our study has revealed the imbalance between development and wound
345 regeneration in the skin blisters. In contrast to wound healing in adult skin, where
346 embryonic programs are reactivated, blister repair during development temporarily
347 inhibits the Wnt pathway, a crucial skin morphogenic driver, leading to the biased
348 activities of HF junctional stem cells from HF morphogenesis towards wound healing.
349 Our findings of the healing processes pave the way for tailored therapeutic interventions
350 for epidermolysis bullosa, pemphigoid diseases and other blistering diseases.

351 **Material and Methods**

352 **Animals**

353 C57BL/6 strain mice were purchased from Clea (Tokyo, Japan). Ins-Topgal+ mice
354 were obtained from RIKEN BRC (Tsukuba, Japan) (58). K14CreER, Lrig1CreER,
355 and R26R-confetti mice were purchased from the Jackson Laboratory (Bar Harbor,
356 Maine, USA). R26R-H2B-mCherry mice were provided by RIKEN (Kobe, Japan).
357 *Col17a1*$^{-/-}$ and hCOL17+;*Col17a1*$^{-/-}$ mice were generated as previously described
358 (34). *Col7a1*$^{-/-}$ mice were provided by Prof. Jouni Uitto (40). The institutional review
359 board of the Hokkaido University Graduate School of Medicine approved all animal
360 studies described below.

361

362 **Suction blisters**

363 Suction blisters were produced on the neonatal murine dorsal skin (P1) using a syringe
364 and connector tubes. The negative pressure applied to the skin (generally for minutes)
365 was 523.4±1.3 mmHg (evaluated by an Ex Pocket Pressure Indicator PM-281 (AS
366 ONE, Osaka, Japan)). The diameter of the syringe attached to the skin was 4 mm. The
367 size of the typical blister was 3 mm in diameter.

368

369 **Histology**

370 Mouse dorsal skin specimens were fixed in formalin and embedded in paraffin after
371 dehydration or were frozen on dry ice in an optimal cutting temperature (OCT)
372 compound. Frozen sections were fixed with 4% paraformaldehyde (PFA) or cold
373 acetone or were stained without fixation. Antigen retrieval with pH 6.0 (citrate) or pH 9.0

374 (EDTA) buffer was performed on deparaffinized sections. Sections were incubated with
375 primary antibodies overnight at 4°C. After being washed in phosphate-buffered saline
376 (PBS), the sections were incubated with secondary antibodies conjugated to FITC,
377 Alexa 488, Alexa 647 or Alexa 680 for 1 hr at room temperature (RT). The nuclei were
378 stained with propidium iodide (PI) or 4',6-diamidino-2-phenylindole (DAPI). The stained
379 immunofluorescent samples were observed using a confocal laser scanning microscope
380 (FV-1000 (Olympus, Tokyo, Japan) or LSM-710 (Zeiss, Oberkochen, Germany)).
381 For immunohistochemistry, horseradish peroxidase (HRP)-tagged secondary
382 antibodies were used. Sections were blocked with hydrogen peroxide, labeled with
383 antibodies, and counterstained with hematoxylin. For morphological analysis,
384 deparaffinized sections were stained with hematoxylin and eosin (H&E) by conventional
385 methods. Alkaline phosphatase staining was performed using a StemAb Alkaline
386 Phosphatase Staining Kit II (Stemgent, San Diego, California, USA). Images of
387 immunohistochemistry, and H&E- and alkaline phosphatase-stained sections were
388 captured with a BZ-9000 microscope (Keyence, Tokyo, Japan).
389 For whole-mount staining, mouse dorsal skin samples were fixed with 4% PFA and
390 immunolabeled or stained with the Alkaline Phosphatase Staining Kit II. For X-gal
391 staining of ins-Topgal+ mouse skin, a beta-galactosidase staining kit (Takara-bio, Shiga,
392 Japan) was used according to the provider’s protocol. Briefly, dorsal skin samples were
393 fixed with 4% PFA for 1 hr at 4°C and soaked in staining solution overnight at RT.
394 Tissues were mounted in a Mowiol solution. Images were observed with LSM-710, FV-
395 1000 or BZ-9000 microscopes.

396 HF morphological stages were evaluated as previously described (28). The length of
397 the major axis of keratinocytes in the intact and regenerated epidermis was measured
398 using ImageJ (NIH, Bethesda, Maryland, USA) on K14-stained sections. The
399 quantification of the cells expressing a particular marker was performed as previously
400 described (59).
401

402 **Antibodies**

403 The following antibodies were used: anti-BrdU (Abcam, Cambridge, UK; BU1/75, Dako;
404 M0744), anti-loricrin (Covance, Princeton, New Jersey, USA), FITC-conjugated anti-
405 CD3e (BioLegend, San Diego, California, USA; 145-2C11), Alexa Fluor 488-conjugated
406 anti-F4/80 (Affymetrix, Santa Clara, California, USA; BM8), FITC (fluorescein
407 isothiocyanate)-conjugated anti-Ly-6G (Beckman Coulter, Brea, California, USA; RB6-
408 8C5), anti-COL4 (Novus Biologicals, Centennial, Colorado; NB120-6586), anti-COL7
409 (homemade (60)), anti- COL17 (Abcam; ab186415), anti-ITGA5 (Abcam; EPR7854),
410 anti-ITGA6 (BD Biosciences Pharmingen, San Diego, California, USA; GoH3), anti-L332
411 (Abcam; ab14509), anti-laminin β1 (Abcam; ab44941), anti-pan-cytokeratin (PROGEN,
412 Wieblingen, Heidelberg, Germany; PRGN-10550), anti-cytokeratin 10 (Biolegend;
413 Poly19054), anti-cytokeratin 14 (ThermoFisher, Waltham, Massachusetts, USA; LL002).
414

415 **BrdU labeling**

416 For proliferation analysis, 10 μg of BrdU (BD Biosciences Pharmingen) per head was
417 intraperitoneally administered 4 hr before sacrifice.
418

419 **Transmission electron microscopy**

420 The samples were taken from C57BL/6 mouse dorsal skin (P1) just after suction
421 blistering was performed. The samples were fixed in 5% glutaraldehyde solution,
422 postfixed in 1% OsO_4, dehydrated, and embedded in Epon 812. The embedded
423 samples were sectioned at 1 μm thickness for light microscopy and thin-sectioned for
424 electron microscopy (70 nm thick). The thin sections were stained with uranyl acetate
425 and lead citrate and examined by transmission electron microscopy (H-7100; Hitachi,
426 Tokyo, Japan).

427

428 **Lineage tracing**

429 K14CreER:R26R-H2B-mCherry, Lrig1CreER:R26R-H2B-mCherry, K14CreER:R26R-
430 confetti, and Lrig1CreER:R26R-confetti mice were intraperitoneally treated with 0.5 mg
431 of tamoxifen (T5648; Sigma-Aldrich, St. Louis, Missouri, USA) at P0. The dorsal skin
432 samples were harvested four days later (P4).

433

434 **RNA sequencing and analysis**

435 Suction-blistered and control samples were collected at P2 and treated with 0.25%
436 trypsin EDTA overnight at 4°C. The epidermis was minced with a scalpel and
437 suspended in 10% FCS DMEM. The cell suspension was filtered through a 70 μm filter,
438 and cell pellets were collected. Library preparation was performed using an Illumina
439 TruSeq RNA prep kit by following the manufacturer's instructions. Briefly, following
440 TRIzol extraction and chemical fragmentation, mRNA was purified with oligo-dT-
441 attached magnetic beads and reverse transcribed into cDNA. Following a second strand

442 synthesis step with DNA polymerase I and RNAse H, the resulting cDNA was subjected
443 to end repair, A-tailing, and Illumina compatible adaptor ligation. Following purification
444 and PCR-mediated enrichment, libraries were purified with AMPure XP beads and
445 sequenced on a NextSeq 500 Illumina sequencer.

446 After quality controls were performed, the raw reads were aligned to the NCBIm37
447 mouse reference genome (mm9) using HiSat2 (61) (version 2.0.0) using options -N 1 -L
448 20 -i S, 1, 0.5 -D 25 -R 5 --pen-noncansplice 20 --mp 1, 0 --sp 3, 0 and providing a list of
449 known splice sites. Expression levels were quantified using featureCounts (62) with
450 RefSeq gene annotation and normalized as TPM using custom scripts. Differential
451 expression analysis was performed using the edgeR (63) software package. After lowly
452 expressed genes (1 count per million in less than two samples) were filtered out, the
453 treatment and control groups were compared using the exact test method (63). Genes
454 with an absolute log2-fold change greater than 1 and false discovery rate (FDR) less
455 than or equal to 0.05 were considered differentially expressed. Hierarchical clustering of
456 gene expression profiles was performed on differentially expressed genes using only
457 Euclidean distances and the complete linkage method. TPM values were normalized as
458 Z-scores across samples, and the distances were computed. GO term and KEGG
459 enrichment analysis on the differentially expressed genes were performed with Enrich
460 (64).

461

462 **Intrablister administration**

463 Ten microliters of 1.8 or 9.0 mM $CaCl_2$ in PBS was administered by syringe into the
464 blisters just after the suction blistering procedure was performed.

465

466 **Statistics**

467 Statistical analyses were performed using GraphPad Prism (GraphPad Software, La
468 Jolla, California, USA). P-values were determined using Student's t-test or one-way
469 ANOVA followed by Tukey's test. P-values are indicated as *0.01<p<0.05,
470 **0.001<p<0.01, ***0.0001<p<0.001, and ****p<0.0001. The values were shown as the
471 means ± standard errors (SE), violin plots or connected with lines showing individual
472 mice.

473

474 **Mathematical modeling**

475 A mathematical model proposed for epidermal cell dynamics (45) was adapted to
476 simulate epidermal wound healing. In this model, epidermal basal cells were
477 represented as spherical particles, with the cell diameter set to 10 μm. Cells designated
478 as epidermal SCs and their progeny could undergo division on the basement
479 membrane. Cell division was described as a process of two initially completely
480 overlapping particles gradually separating into two distinct particles. When a newly
481 created cell was not fully surrounded by other cells, it was judged as being in a
482 regeneration process and immediately underwent a transition to an oblate spheroid
483 shape with the long axis increased by a factor of 2 (normal) or 1.5 (simulating *Col7a1*$^{-/-}$
484 and Ca-treated blisters) while its volume was kept constant. The same division rate was
485 assigned to all proliferative cells, with an average division period of 57.6 [arb. unit].
486 Forces exerted on a cell came from adhesion and excluded-volume interactions with
487 other cells and with the basement membrane. SCs were tightly bound and unable to

488 detach from the basement membrane, while the progeny were weakly bound so that
489 they could detach from the membrane via the ambient pressure: the detached cells
490 were removed from the system. The basement membrane was assumed to be a rigid
491 flat surface, whose shape remained unchanged over time. These interactions were
492 calculated to obtain the time evolution of the whole system by solving equations given in
493 a previous report (45). The simulation region was set to 600 μm x 600 μm horizontally
494 with periodic boundary conditions. To prepare the initial conditions for the simulation of
495 subepidermal blister healing, we first ran a simulation with SCs placed on the basement
496 membrane until their progeny covered the whole surface. Then, we set the progeny to
497 be nonproliferative and created epidermal defects by removing the cells that were inside
498 a disk domain with a diameter of 480 μm.

499 The number of HFs in humans was estimated from the data in Supplementary
500 Table 1 under the assumption that HFs were uniformly distributed and that the number
501 of proliferative cells per HF was proportional to the volume of the HF. Using the mean
502 values of the data, we estimated that the ratio of human to mouse proliferative cells in
503 epidermal defects is 0.174:1. The initial number of cells was prepared accordingly in the
504 simulations of human epidermal defects.

505

506 **Human samples**

507 From the H&E-stained skin of patients with congenital or autoimmune subepidermal
508 blistering diseases (73 EB or 188 bullous pemphigoid (BP) samples, respectively), the
509 samples that met the following histological criteria were selected: (1) subepidermal
510 blisters or a skin split at the dermoepidermal junction; (2) re-epithelization in the area;

511 and (3) presence of HFs on the blister base. Three BP samples fulfilled all the criteria
512 (blisters 1, 2, and 3) and were observed with a Keyence BZ-9000 microscope. The
513 institutional review board of the Hokkaido University Graduate School of Medicine
514 approved all human studies described above (ID: 13-043 and 15-052). The study was
515 conducted according to the Declaration of Helsinki Principles. Participants or their legal
516 guardians provided written informed consent.
517

518 **Author contributions**

519 Y. F. designed and performed the experiments, analyzed the data, interpreted the
520 results, and wrote the manuscript. M. W., S. T., H. N., H. K., Y. W., Y. M, A. L., V. P., H.
521 U., H. I., W. N., and S. O. performed the experiments and analyzed the data. K. O., Y.
522 K., and M. N. performed the mathematical modeling and wrote the manuscript. G. D.
523 designed and performed the experiments, analyzed the data and interpreted the results.
524 S. H. interpreted the results and supervised the study. K. N. conceived and designed
525 the experiments, analyzed the data, interpreted the results, wrote the manuscript and
526 supervised the study.
527

528 **Acknowledgments**

529 We thank Ms. Meari Yoshida for her technical assistance. We also thank Professor
530 Yumiko Saga, Professor Kim B Yancey, and Professor Jouni Uitto for providing the ins-
531 Topgal+, K14-hCOL17, and *Col7a1*$^{-/-}$ mice, respectively. This work was funded by
532 AMED (ID: 18059057), JSPS (KAKEN 17K16317), the Uehara Foundation, the Lydia
533 O'Leary Memorial Pias Dermatological Foundation to KN, JST CREST (JPMJCR15D2)

534 to MN, JSPS (KAKEN 16K10120) to HN, AIRC IG 20240 to SO, and AIRC MFAG 2018
535 (ID: 21640) to GD.
536

537 **References**

538 1. Miao Q*, et al.* (2019) SOX11 and SOX4 drive the reactivation of an embryonic
539 gene program during murine wound repair. *Nat Commun* 10(1):4042.
540 2. Fernandez Vallone V*, et al.* (2016) Trop2 marks transient gastric fetal epithelium
541 and adult regenerating cells after epithelial damage. *Development* 143(9):1452-
542 1463.
543 3. Yui S*, et al.* (2018) YAP/TAZ-Dependent Reprogramming of Colonic Epithelium
544 Links ECM Remodeling to Tissue Regeneration. *Cell Stem Cell* 22(1):35-49 e37.
545 4. Nusse YM*, et al.* (2018) Parasitic helminths induce fetal-like reversion in the
546 intestinal stem cell niche. *Nature* 559(7712):109-113.
547 5. Natsuga K (2014) Epidermal barriers. *Cold Spring Harb Perspect Med*
548 4(4):a018218.
549 6. Donati G & Watt FM (2015) Stem cell heterogeneity and plasticity in epithelia.
550 *Cell Stem Cell* 16(5):465-476.
551 7. McMillan JR, Akiyama M, & Shimizu H (2003) Epidermal basement membrane
552 zone components: ultrastructural distribution and molecular interactions. *J*
553 *Dermatol Sci* 31(3):169-177.
554 8. Watt FM & Fujiwara H (2011) Cell-extracellular matrix interactions in normal and
555 diseased skin. *Cold Spring Harb Perspect Biol* 3(4).
556 9. Niculescu C*, et al.* (2011) Conditional ablation of integrin alpha-6 in mouse
557 epidermis leads to skin fragility and inflammation. *Eur J Cell Biol* 90(2-3):270-
558 277.

559 10. Brakebusch C*, et al.* (2000) Skin and hair follicle integrity is crucially dependent
560 on beta 1 integrin expression on keratinocytes. *EMBO J* 19(15):3990-4003.
561 11. Watanabe M*, et al.* (2017) Type XVII collagen coordinates proliferation in the
562 interfollicular epidermis. *Elife* 6.
563 12. Rognoni E & Watt FM (2018) Skin Cell Heterogeneity in Development, Wound
564 Healing, and Cancer. *Trends Cell Biol* 28(9):709-722.
565 13. Dekoninck S & Blanpain C (2019) Stem cell dynamics, migration and plasticity
566 during wound healing. *Nat Cell Biol* 21(1):18-24.
567 14. Garcin CL, Ansell DM, Headon DJ, Paus R, & Hardman MJ (2016) Hair Follicle
568 Bulge Stem Cells Appear Dispensable for the Acute Phase of Wound Re-
569 epithelialization. *Stem Cells* 34(5):1377-1385.
570 15. Chetty BV, Boissy RE, Warden GD, & Nordlund JJ (1992) Basement membrane
571 and fibroblast aberration in blisters at the donor, graft, and spontaneously healed
572 sites in patients with burns. *Arch Dermatol* 128(2):181-186.
573 16. Vahidnezhad H, Youssefian L, Saeidian AH, & Uitto J (2019) Phenotypic
574 Spectrum of Epidermolysis Bullosa: The Paradigm of Syndromic versus Non-
575 Syndromic Skin Fragility Disorders. *J Invest Dermatol* 139(3):522-527.
576 17. Fine JD*, et al.* (2014) Inherited epidermolysis bullosa: updated recommendations
577 on diagnosis and classification. *J Am Acad Dermatol* 70(6):1103-1126.
578 18. Schmidt E & Zillikens D (2013) Pemphigoid diseases. *Lancet* 381(9863):320-332.
579 19. White KD*, et al.* (2018) SJS/TEN 2017: Building Multidisciplinary Networks to
580 Drive Science and Translation. *J Allergy Clin Immunol Pract* 6(1):38-69.

581 20. Park S*, et al.* (2017) Tissue-scale coordination of cellular behaviour promotes
582 epidermal wound repair in live mice. *Nat Cell Biol* 19(2):155-163.
583 21. Gonzales KAU & Fuchs E (2017) Skin and Its Regenerative Powers: An Alliance
584 between Stem Cells and Their Niche. *Dev Cell* 43(4):387-401.
585 22. Donati G*, et al.* (2017) Wounding induces dedifferentiation of epidermal Gata6(+)
586 cells and acquisition of stem cell properties. *Nat Cell Biol* 19(6):603-613.
587 23. Aragona M*, et al.* (2017) Defining stem cell dynamics and migration during
588 wound healing in mouse skin epidermis. *Nat Commun* 8:14684.
589 24. Page ME, Lombard P, Ng F, Gottgens B, & Jensen KB (2013) The epidermis
590 comprises autonomous compartments maintained by distinct stem cell
591 populations. *Cell Stem Cell* 13(4):471-482.
592 25. Kiistala U & Mustakallio KK (1967) Dermo-epidermal separation with suction.
593 Electron microscopic and histochemical study of initial events of blistering on
594 human skin. *J Invest Dermatol* 48(5):466-477.
595 26. Kiistala U & Mustakallio KK (1964) In-Vivo Separation of Epidermis by Production
596 of Suction Blisters. *Lancet* 2(7348):1444-1445.
597 27. Krawczyk WS (1971) A pattern of epidermal cell migration during wound healing.
598 *J Cell Biol* 49(2):247-263.
599 28. Paus R*, et al.* (1999) A comprehensive guide for the recognition and
600 classification of distinct stages of hair follicle morphogenesis. *J Invest Dermatol*
601 113(4):523-532.
602 29. Liu N*, et al.* (2019) Stem cell competition orchestrates skin homeostasis and
603 ageing. *Nature*.

604 30. Matsumura H*, et al.* (2016) Hair follicle aging is driven by transepidermal
605 elimination of stem cells via COL17A1 proteolysis. *Science* 351(6273):aad4395.
606 31. Tanimura S*, et al.* (2011) Hair follicle stem cells provide a functional niche for
607 melanocyte stem cells. *Cell Stem Cell* 8(2):177-187.
608 32. Natsuga K, Watanabe M, Nishie W, & Shimizu H (2019) Life before and beyond
609 blistering: The role of collagen XVII in epidermal physiology. *Exp Dermatol*
610 28(10):1135-1141.
611 33. McGrath JA*, et al.* (1995) Mutations in the 180-kD bullous pemphigoid antigen
612 (BPAG2), a hemidesmosomal transmembrane collagen (COL17A1), in
613 generalized atrophic benign epidermolysis bullosa. *Nat Genet* 11(1):83-86.
614 34. Nishie W*, et al.* (2007) Humanization of autoantigen. *Nat Med* 13(3):378-383.
615 35. Watanabe M, Natsuga K, Shinkuma S, & Shimizu H (2018) Epidermal aspects of
616 type VII collagen: Implications for dystrophic epidermolysis bullosa and
617 epidermolysis bullosa acquisita. *J Dermatol* 45(5):515-521.
618 36. Shimizu H*, et al.* (1997) Most anchoring fibrils in human skin originate and
619 terminate in the lamina densa. *Lab Invest* 76(6):753-763.
620 37. Hilal L*, et al.* (1993) A homozygous insertion-deletion in the type VII collagen
621 gene (COL7A1) in Hallopeau-Siemens dystrophic epidermolysis bullosa. *Nat*
622 *Genet* 5(3):287-293.
623 38. Christiano AM*, et al.* (1993) A missense mutation in type VII collagen in two
624 affected siblings with recessive dystrophic epidermolysis bullosa. *Nat Genet*
625 4(1):62-66.

626 39. Nystrom A*, et al.* (2013) Collagen VII plays a dual role in wound healing. *J Clin*
627 *Invest* 123(8):3498-3509.
628 40. Heinonen S*, et al.* (1999) Targeted inactivation of the type VII collagen gene
629 (Col7a1) in mice results in severe blistering phenotype: a model for recessive
630 dystrophic epidermolysis bullosa. *J Cell Sci* 112 (Pt 21):3641-3648.
631 41. Chen M*, et al.* (2002) Restoration of type VII collagen expression and function in
632 dystrophic epidermolysis bullosa. *Nat Genet* 32(4):670-675.
633 42. Chen M*, et al.* (2000) Development and characterization of a recombinant
634 truncated type VII collagen "minigene". Implication for gene therapy of dystrophic
635 epidermolysis bullosa. *J Biol Chem* 275(32):24429-24435.
636 43. Magee AI, Lytton NA, & Watt FM (1987) Calcium-induced changes in
637 cytoskeleton and motility of cultured human keratinocytes. *Exp Cell Res*
638 172(1):43-53.
639 44. Hennings H*, et al.* (1980) Calcium regulation of growth and differentiation of
640 mouse epidermal cells in culture. *Cell* 19(1):245-254.
641 45. Kobayashi Y*, et al.* (2018) Interplay between epidermal stem cell dynamics and
642 dermal deformation. *npj Computational Materials* 4(1):45.
643 46. Kobayashi Y, Sawabu Y, Kitahata H, Denda M, & Nagayama M (2016)
644 Mathematical model for calcium-assisted epidermal homeostasis. *J Theor Biol*
645 397:52-60.
646 47. Osaka N*, et al.* (2007) ASK1-dependent recruitment and activation of
647 macrophages induce hair growth in skin wounds. *J Cell Biol* 176(7):903-909.

648 48. Ito M, *et al.* (2007) Wnt-dependent de novo hair follicle regeneration in adult
649 mouse skin after wounding. *Nature* 447(7142):316-320.
650 49. Rognoni E, *et al.* (2016) Inhibition of beta-catenin signalling in dermal fibroblasts
651 enhances hair follicle regeneration during wound healing. *Development*
652 143(14):2522-2535.
653 50. Lane EB, Wilson CA, Hughes BR, & Leigh IM (1991) Stem cells in hair follicles.
654 Cytoskeletal studies. *Ann N Y Acad Sci* 642:197-213.
655 51. Hertle MD, Kubler MD, Leigh IM, & Watt FM (1992) Aberrant integrin expression
656 during epidermal wound healing and in psoriatic epidermis. *J Clin Invest*
657 89(6):1892-1901.
658 52. Leivo T, *et al.* (2000) Re-epithelialization rate and protein expression in the
659 suction-induced wound model: comparison between intact blisters, open wounds
660 and calcipotriol-pretreated open wounds. *Br J Dermatol* 142(5):991-1002.
661 53. Chen X, *et al.* (2019) IL-17R-EGFR axis links wound healing to tumorigenesis in
662 Lrig1(+) stem cells. *J Exp Med* 216(1):195-214.
663 54. Tang DD & Gerlach BD (2017) The roles and regulation of the actin cytoskeleton,
664 intermediate filaments and microtubules in smooth muscle cell migration. *Respir*
665 *Res* 18(1):54.
666 55. Uroz M, *et al.* (2019) Traction forces at the cytokinetic ring regulate cell division
667 and polyploidy in the migrating zebrafish epicardium. *Nat Mater* 18(9):1015-1023.
668 56. Paladini RD, Takahashi K, Bravo NS, & Coulombe PA (1996) Onset of re-
669 epithelialization after skin injury correlates with a reorganization of keratin

670 filaments in wound edge keratinocytes: defining a potential role for keratin 16. *J*
671 *Cell Biol* 132(3):381-397.
672 57. Tosti A, Duque-Estrada B, & Murrell DF (2010) Alopecia in epidermolysis bullosa.
673 *Dermatol Clin* 28(1):165-169.
674 58. Moriyama A*, et al.* (2007) GFP transgenic mice reveal active canonical Wnt
675 signal in neonatal brain and in adult liver and spleen. *Genesis* 45(2):90-100.
676 59. Natsuga K, Cipolat S, & Watt FM (2016) Increased Bacterial Load and
677 Expression of Antimicrobial Peptides in Skin of Barrier-Deficient Mice with
678 Reduced Cancer Susceptibility. *J Invest Dermatol* 136(1):99-106.
679 60. Iwata H*, et al.* (2013) B cells, dendritic cells, and macrophages are required to
680 induce an autoreactive CD4 helper T cell response in experimental epidermolysis
681 bullosa acquisita. *J Immunol* 191(6):2978-2988.
682 61. Kim D, Langmead B, & Salzberg SL (2015) HISAT: a fast spliced aligner with low
683 memory requirements. *Nat Methods* 12(4):357-360.
684 62. Liao Y, Smyth GK, & Shi W (2014) featureCounts: an efficient general purpose
685 program for assigning sequence reads to genomic features. *Bioinformatics*
686 30(7):923-930.
687 63. Robinson MD, McCarthy DJ, & Smyth GK (2010) edgeR: a Bioconductor
688 package for differential expression analysis of digital gene expression data.
689 *Bioinformatics* 26(1):139-140.
690 64. Kuleshov MV*, et al.* (2016) Enrichr: a comprehensive gene set enrichment
691 analysis web server 2016 update. *Nucleic Acids Res* 44(W1):W90-97.
692

Figure 1. Healing of subepidermal blisters in neonatal mice

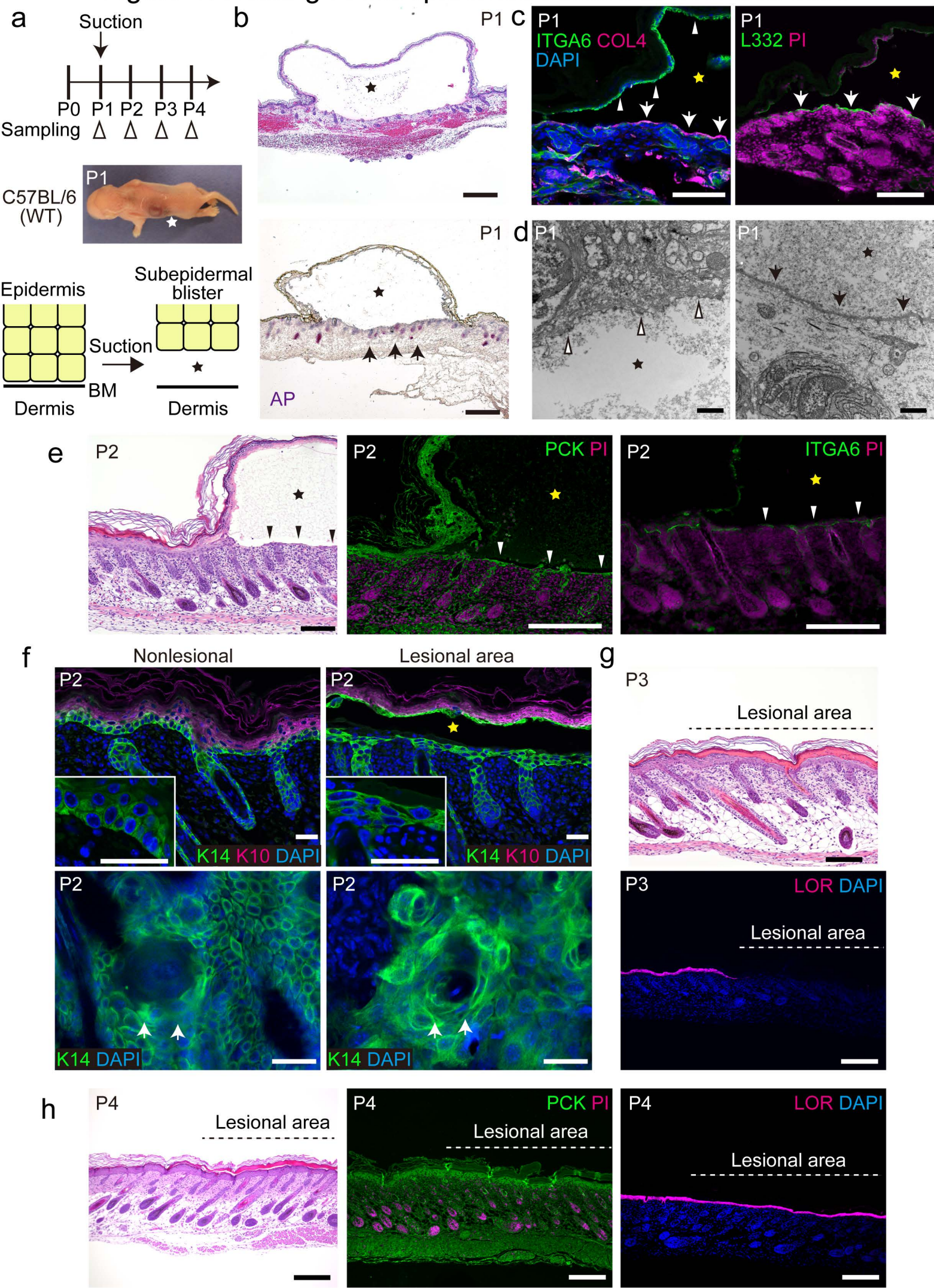

693 **Figure legends**

694 **Figure 1. Healing of subepidermal blisters in neonatal mice.**

695 (a) Schematic diagram of suction blistering and sample collection. A blister produced on
696 C57BL/6 wild-type (WT) mouse dorsal skin at P1. BM: basement membrane. (b-d)
697 Blistered samples at P1. Hematoxylin and eosin (H&E) and alkaline phosphatase (AP)
698 staining (b). Hair follicles (HFs) remaining in the dermis (indicated by arrows). Scale bar:
699 500 μm. α6 Integrin (ITGA6, indicated by arrowheads) and type IV collagen (COL4,
700 arrows) labeling (c, left). Laminin 332 (L332, arrows) staining (c, right). Scale bar:
701 100 μm. Ultrastructural findings of blistered skin (left image: blister roof, right image:
702 blister bottom) (d). Hemidesmosomes (white arrowheads) and lamina densa (arrows)
703 are indicated. Scale bar: 1 μm. (e) H&E, pan-cytokeratin (PCK), and ITGA6 staining at
704 P2. The regenerated epidermis is indicated by arrowheads. Scale bar: 200 μm. (f)
705 Keratin 14 (K14) and keratin 10 (K10) staining of the nonlesional (intact) and lesional
706 (blistered) skin at P2 (upper images and inlets: sections, lower images: whole-mount
707 imaging). HFs are indicated by arrows in the whole-mount images. Scale bar: 30 μm. (g)
708 H&E and loricrin (LOR) staining at P3. Scale bar: 200 μm. (h) H&E, PCK, and LOR
709 staining at P4. Scale bar: 200 μm. Blisters are indicated by stars.

710

711

Figure 2. Delayed HF development during subepidermal blister healing

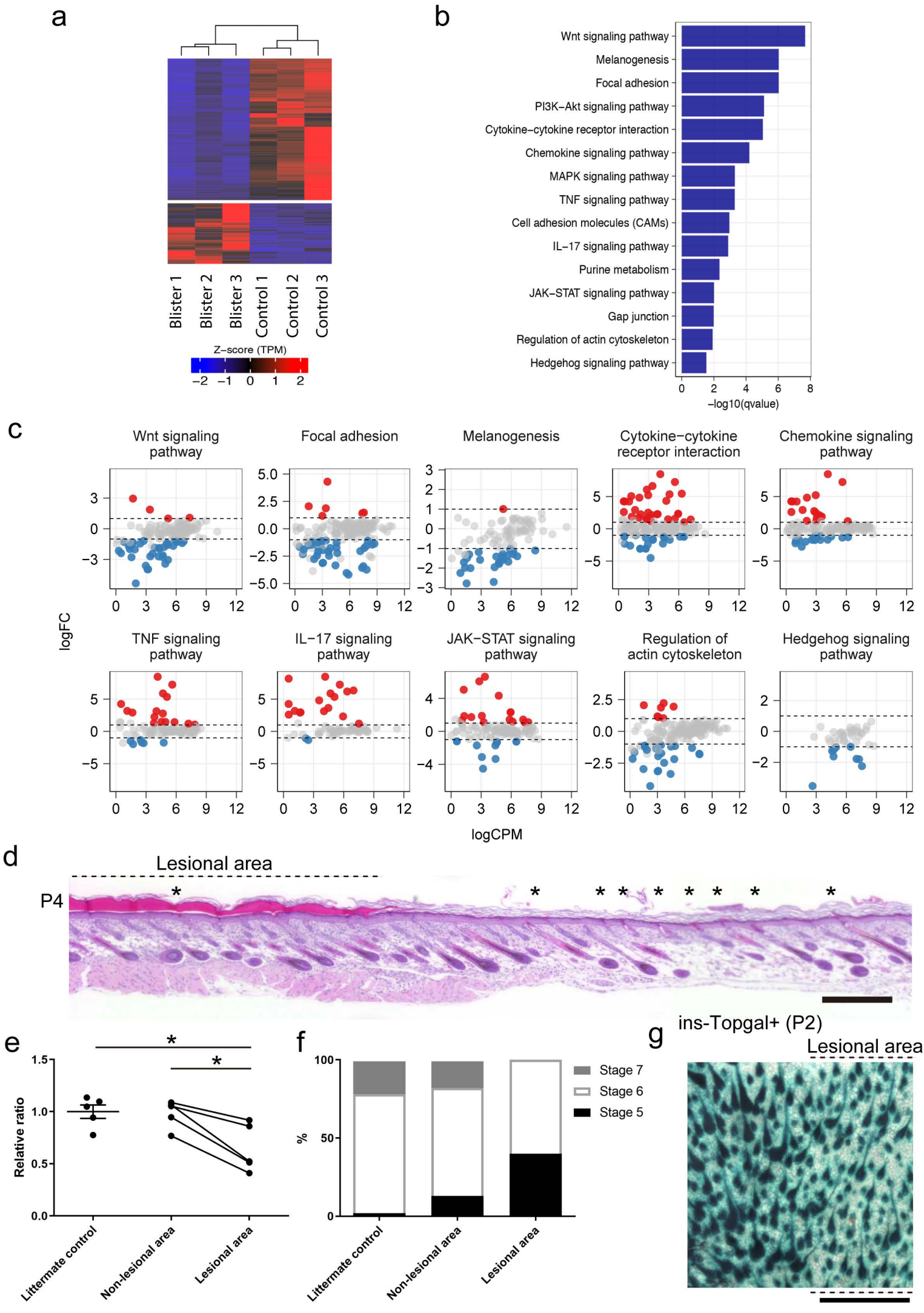

712 **Figure 2. Delayed HF growth during subepidermal blister healing.**

713 (a) Heat map (Pearson's correlation) of differentially expressed genes between the
714 blistered (regenerated) and control WT dorsal skin epidermis at P2 (n=3). (b) GO
715 analysis of differentially expressed genes in the regenerated epidermis. (c) Scatter plots
716 of differentially expressed genes in the regenerated epidermis. (d) Hair canals in the
717 regenerated (lesional) and nonlesional epidermis at P4 (indicated by asterisks). Scale
718 bar: 300 μm. (e) Quantification of hair canals in the lesional, nonlesional, and unaffected
719 littermate control epidermis at P4 (n=5). The data are shown as the mean ± SE
720 (littermate control) or connected with lines showing individual mice. *$0.01<p<0.05$, one-
721 way ANOVA test, followed by Tukey's test. (f) HF morphogenesis stages at P4 in
722 lesional, nonlesional, and unaffected littermate control skin (n=5). (g) Whole-mount
723 imaging of the blistered skin of ins-Topgal+ mice at P2. Scale bar: 500 μm.

724

725

Figure 3. Predominant contribution of HF-derived keratinocytes to subepidermal blister healing

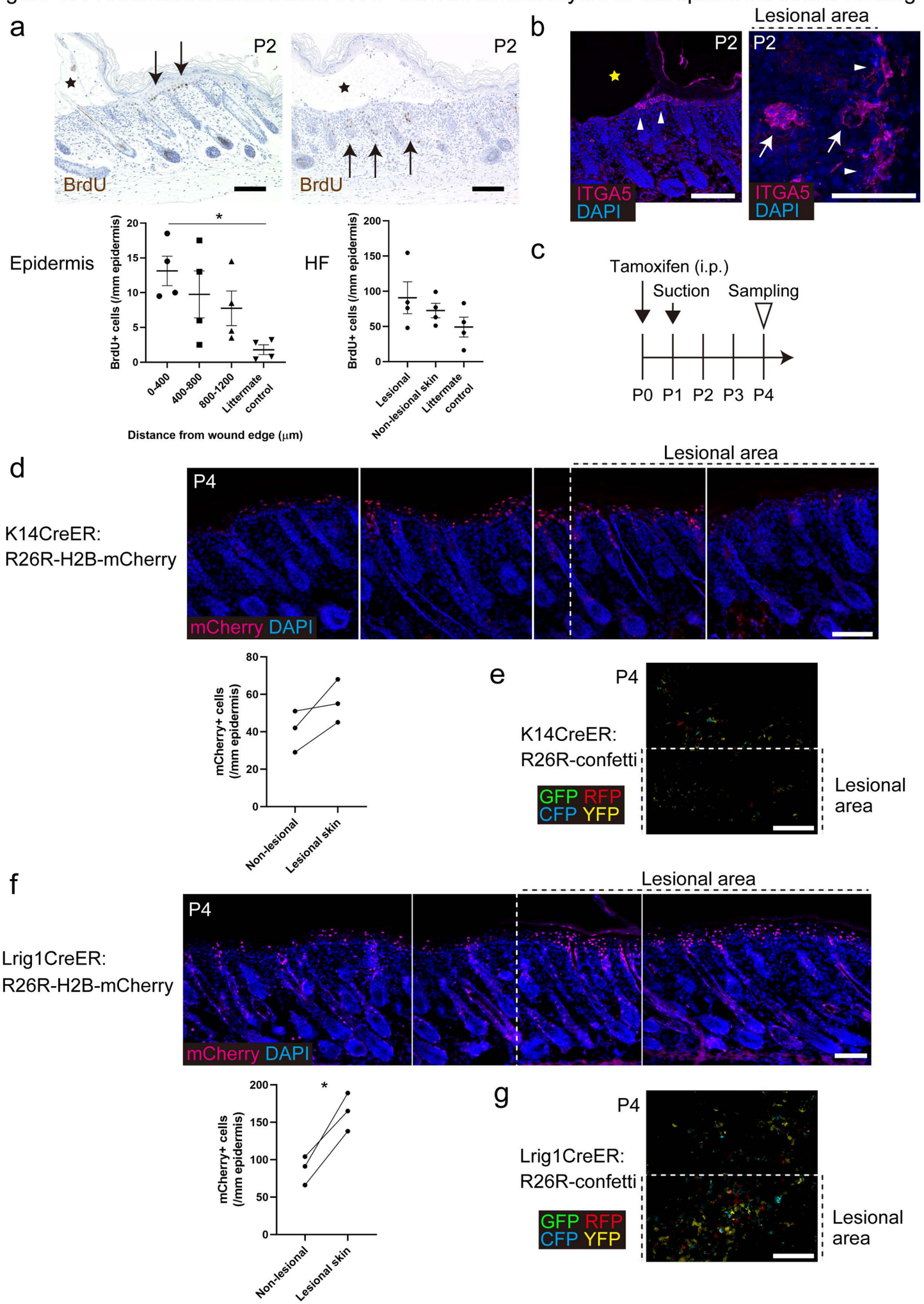

726 **Figure 3. Predominant contribution of HF-derived keratinocytes to subepidermal**
727 **blister healing.**
728 (a) BrdU labeling of blistered samples at P2. Scale bar: 100 μm. BrdU-positive cells are
729 indicated by arrows. Quantification of BrdU-positive cells in the epidermis and HFs
730 (n=4). The data are shown as the mean ± SE. *0.01<p<0.05, one-way ANOVA test,
731 followed by Tukey's test. (b) α5 integrin (ITGA5) labeling at P2 (left image: section, right
732 image: whole-mount). Scale bar: 100 μm. Blister edges (epidermal tongue) and HFs are
733 indicated by arrowheads and arrows, respectively. Blisters are indicated by stars. (c)
734 Lineage tracing strategy. (d) Sections of K14CreER:H2B-mCherry mice at P4.
735 Quantification of mCherry-positive cells (n=3). Scale bar: 100 μm. The data from
736 individual mice are connected by lines. Student's t-test. (e) Whole-mount imaging of
737 K14CreER:R26R-confetti samples at P4. Scale bar: 200 μm. (f) Sections of
738 Lrig1CreER:H2B-mCherry mouse skin at P4. Quantification of mCherry-positive cells
739 (n=3). Scale bar: 100 μm. The data from individual mice are connected by lines.
740 *0.01<p<0.05, Student's t-test. (g) Whole-mount imaging of Lrig1CreER:R26R-confetti
741 mouse samples at P4. Scale bar: 200 μm.
742
743

Figure 4. Effects of HF depletion on subepidermal blister healing

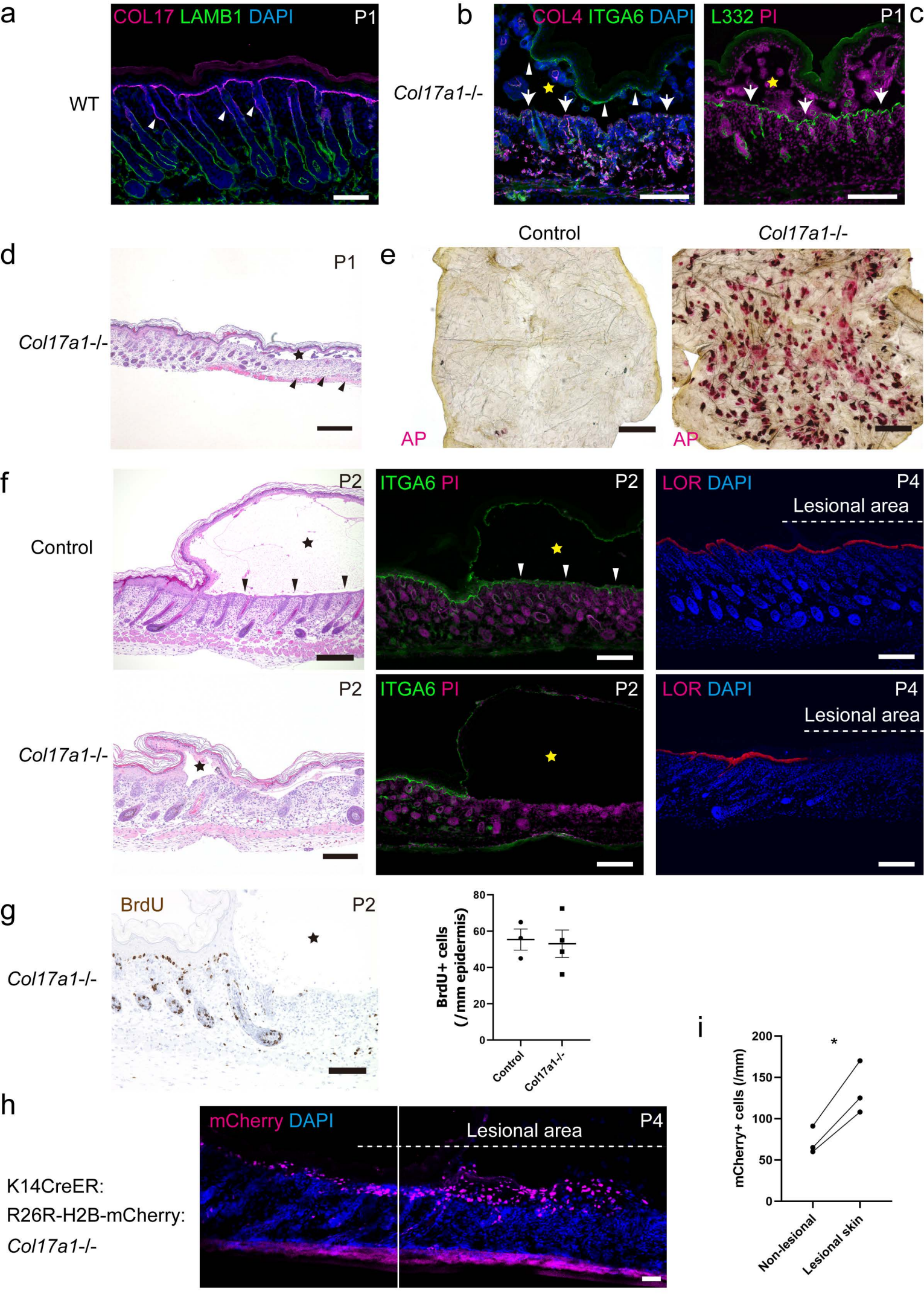

744 **Figure 4. Effects of HF depletion on subepidermal blister healing.**

745 (a) Type XVII collagen (COL17, arrowheads indicate the hair bulge) and laminin β1
746 (LAMB1) labeling in WT dorsal skin sections (P1). Scale bar: 100 μm. (b, c) Blistered
747 samples of *Col17a1*$^{-/-}$ mouse dorsal skin at P1. ITGA6 (indicated by arrowheads) and
748 COL4 (arrows) labeling (b). L332 staining (c, arrows). Scale bar: 100 μm. (d) H&E
749 staining of blistered skin from *Col17a1*$^{-/-}$ mice at P1. HFs detached from the dermis in
750 *Col17a1*$^{-/-}$ skin are indicated by arrowheads. Scale bar: 500 μm. (e) Whole-mount AP
751 staining of the blister roof epidermis from *Col17a1*$^{-/-}$ mice and littermate controls at P1.
752 Scale bar: 500 μm. (f) H&E (P2), ITGA6 (P2) and LOR staining (P4) of *Col17a1*$^{-/-}$ mice
753 and littermate controls. The regenerated epidermis is indicated by arrowheads. Scale
754 bar: 200 μm. (g) BrdU labeling of *Col17a1*$^{-/-}$ skin at P2. Scale bar: 100 μm.
755 Quantification of BrdU-positive cells in the epidermis surrounding blisters (n=4). The
756 data are shown as the mean ± SE. Student's t-test. (h, i) Lineage tracing of
757 K14CreER:R26R-mCherry:*Col17a1*$^{-/-}$ at P4 (h). Scale bar: 100 μm. Quantification of
758 mCherry-positive cells in the regenerated epidermis (n=3) (i). The data from individual
759 mice are connected by lines. *$0.01<p<0.05$, Student's t-test. Blisters are indicated by
760 stars.

761

762

Figure 5. Involvement of keratinocyte shape transformation in subepidermal blister healing

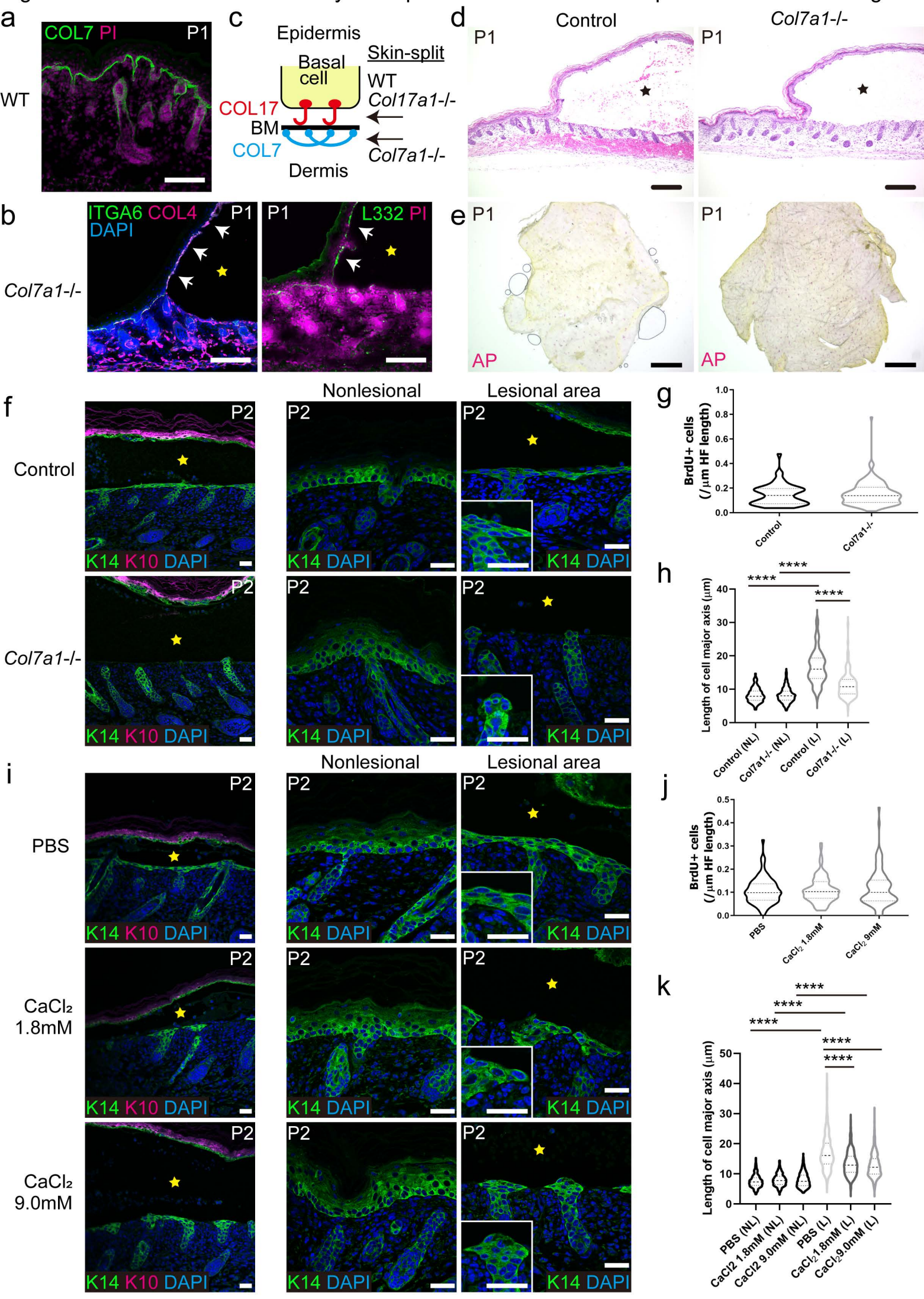

763 **Figure 5. Involvement of keratinocyte shape transformation in subepidermal**
764 **blister healing.**
765 (a) Type VII collagen (COL7) labeling in WT dorsal skin sections (P1). Scale bar:
766 200 μm. (b) ITGA6/COL4 (left, indicated by arrows) and L332 labeling (right, indicated
767 by arrows) in the blistered skin of *Col7a1*$^{-/-}$ mice at P1. Scale bar: 100 μm. (c)
768 Schematic diagram of control, *Col17a1*$^{-/-}$, and *Col7a1*$^{-/-}$ mouse skin splits. BM:
769 basement membrane. (d) H&E staining of blistered skin from *Col7a1*$^{-/-}$ mice and their
770 littermate controls at P1. Scale bar: 200 μm. (e) Whole-mount AP staining of the blister
771 roof epidermis from *Col7a1*$^{-/-}$ mice and their littermate controls at P1. Scale bar: 500 μm.
772 (f) K10/K14 (low magnification) and K14 (high magnification) labeling of *Col7a1*$^{-/-}$ mouse
773 and littermate control blistered skin at P2. Scale bar: 30 μm. (g) Quantification of BrdU-
774 positive cells per μm HF length (n=55 HFs from three control and 143 HFs from four
775 *Col7a1*$^{-/-}$ mice). The data are shown as violin plots. Student's t-test. (h) Length of the
776 major axis of keratinocytes in the regenerated epidermis (n=244 (control, L), and 132
777 (*Col7a1*$^{-/-}$, L) cells from four mice, respectively) and in the surrounding intact epidermis
778 (basal cells; n=200 (control, NL), 299 (*Col7a1*$^{-/-}$, NL), from four mice, respectively). NL:
779 nonlesional area. L: lesional area. The data are shown as violin plots. ****$p<0.0001$,
780 one-way ANOVA test, followed by Tukey's test. (i) K10/K14 and K14 (high
781 magnification) labeling of WT blistered skin treated with $CaCl_2$ or PBS at P2. Scale bar:
782 30 μm. (j) Quantification of BrdU-positive cells per μm HF length (n=83 (PBS), 95 (1.8
783 mM $CaCl_2$), and 97 (9.0 mM $CaCl_2$) HFs from four mice). (k) Length of the major axis of
784 keratinocytes in the regenerated epidermis (n=433 (PBS, L), 451 (1.8 mM $CaCl_2$, L), and
785 425 (9.0 mM $CaCl_2$, L) cells from four mice) and in the surrounding intact epidermis

786 (basal cells; n=311 (PBS, NL), 279 (1.8 mM $CaCl_2$, NL), 302 (9.0 mM $CaCl_2$, NL) cells
787 from four mice). NL: nonlesional area. L: lesional area. The data are shown as violin
788 plots. ****$p<0.0001$, one-way ANOVA test, followed by Tukey's test. Blisters are
789 indicated by stars.
790
791

Figure 6. Mathematical modeling of subepidermal blister healing

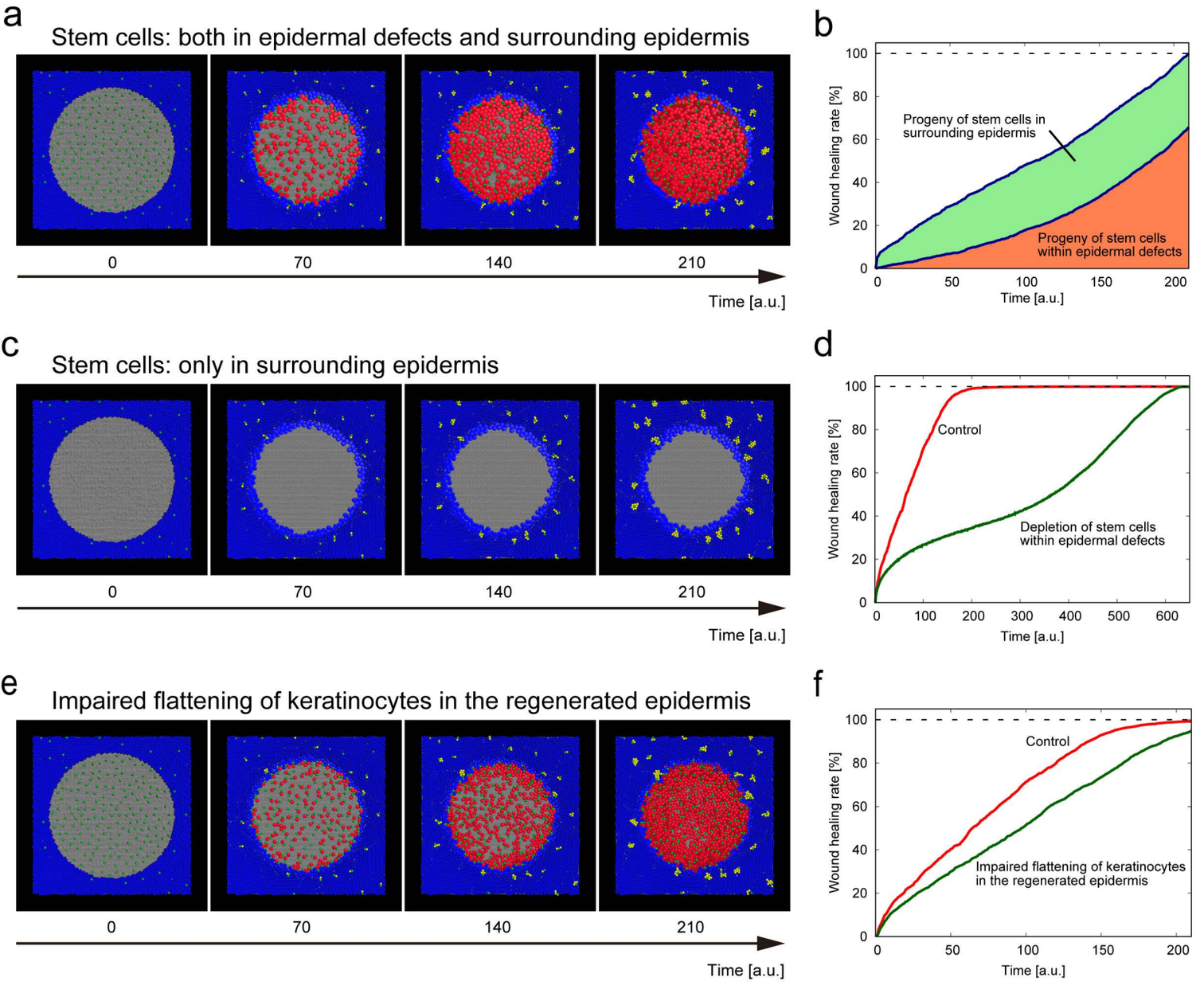

792 **Figure 6. Mathematical modeling of subepidermal blister healing.**

793 (a) A particle-based model of subepidermal blister healing at the basal layer. Epidermal
794 basal cells (colored in blue), which do not divide, are placed on the basement
795 membrane (gray). Stem cells (SCs, green) give rise to progeny (simulating HF-derived
796 cells; red) within epidermal defects or in the surrounding epidermis (IFE-derived cells;
797 yellow). t: arbitrary time. See **Supplementary Video 1**. (b) Contribution of each progeny
798 cell within the epidermal defect or of surrounding epidermis to subepidermal blister
799 healing, measured as the ratio of the area occupied by each progeny to the area of the
800 initial epidermal defect. (c) A model of subepidermal blister healing without SCs within
801 epidermal defects. See **Supplementary Video 2**. (d) Time course of subepidermal
802 blister healing in control (a) and SC-depleted epidermal defects (c). (e) Effects of the
803 impaired flattening of keratinocytes upon epidermal regeneration. The diameter of basal
804 keratinocytes (long axis of the spheroid) in the regenerated vs. surrounding epidermis
805 was calculated as 1.5:1 (in contrast to 2:1 in Figure 6a). See **Supplementary Video 3**.
806 (f) Time course of wound healing for control (a) and less flattened keratinocytes in the
807 regenerated epidermis (e).

808